Letter

Antiferromagnetic Resonances in Superconductor-Ferromagnet Multilayers

I.A. Golovchanskiy[1,2,3,*] V.V. Ryazanov[1,2,4] and V.S. Stolyarov[1,2,3]

[1]*Moscow Institute of Physics and Technology, State University, 9 Institutskiy per., Dolgoprudny, Moscow Region 141700, Russia*
[2]*National University of Science and Technology MISIS, 4 Leninsky prosp., Moscow 119049, Russia*
[3]*Dukhov Research Institute of Automatics (VNIIA), Moscow 127055, Russia*
[4]*Institute of Solid State Physics (ISSP RAS), Chernogolovka, Moscow region 142432, Russia*

In this work, we study the magnetization dynamics in a superconductor-ferromagnet (*S-F*) thin-film multilayer. Theoretical considerations supported by broadband ferromagnetic resonance spectroscopy reveal the development of acoustic and optic resonance modes in *S-F* multilayers at significantly higher frequencies in comparison to the Kittel mode of individual *F* layers. These modes are formed due to antiferromagneticlike interactions between *F* layers via shared circulating superconducting currents in the *S* layers. The gap between resonance modes is determined by the thickness and superconducting penetration depth in the *S* layers. Overall, the rich spectrum of *S-F* multilayers and its tunability may open up wide prospects for application of these multilayers in magnonics as well as in various superconducting hybrid systems.

Introduction.—The hybridization of antagonistic superconducting (*S*) and ferromagnetic (*F*) orders provides various opportunities in electronics and spintronics, which have been repeatedly demonstrated in past decades [1]. Recently, the interest in *S-F* hybridization has been reinforced by demonstrations of its prospects in relation to the phenomena of magnetization dynamics. In particular, interactions between the magnetization dynamics and the superconducting vortex lattice allow to form and guide the tunable magnonic band structure [2], as well as to induce exchange spin waves by means of the dc electric current [3]. Also, interactions between the magnetization dynamics and superconducting Meissner currents in hybrid structures modify the spin-wave dispersion [4,5], which can be used for the creation of magnonic crystals [6] or for the gating of magnon currents [7]. Remarkably, the low speed of electromagnetic propagation in superconductor-insulator-superconductor thin-film structures facilitates the achievement of ultrastrong photon-to-magnon coupling in on-chip hybrid devices [8,9], with the aim of achieving photon-to-magnon entanglement [10].

A new strong phenomenon in *S-F* hybrid structures has been reported recently in Refs. [11–13] and investigated further in Refs. [14,15]. In superconductor-ferromagnet-superconductor (*S-F-S*) thin-film structures, in the presence of electronic interaction between superconducting

and ferromagnetic layers, a radical increase in the ferromagnetic resonance (FMR) frequency occurs. The mechanism behind the phenomenon can be viewed qualitatively as the coupling of magnetization precession in the ferromagnetic layer to the kinetic inductance (i.e., the imaginary conductance) of the superconducting layer at the interface and the formation of macroscopic alternating circulating superconducting currents in the opposite phase to the magnetization precession, which acts as additional magnetic anisotropy and enhances the resonance frequency.

In this work, we generalize the problem and consider the magnetization dynamics in arbitrary *S-F* multilayers. Coupling between ferromagnetic layers via superconducting currents induces antiferromagneticlike interactions between the *F* layers, which result in acoustic and optical resonance modes. Theoretical considerations supported by broadband ferromagnetic resonance spectroscopy demonstrate that the spectrum is determined by the geometrical characteristics of a multilayer as well as by the superconducting penetration depth in the *S* layers.

Theory.—Following Refs. [15–17], the electrodynamics and magnetization dynamics in *S-F* multilayers obeys the conventional Maxwell equations supplemented by Ohm's law with imaginary conductance in superconducting layers and by the Polder susceptibility in ferromagnetic layers. By neglecting edge effects, the *y* component of the magnetic field as well as the *x* components of electric field and

*golov4anskiy@gmail.com

of the current are functions of the transverse coordinate z only (see Fig. 1). Derivation of the magnetic field in the S and F layers from the initial Maxwell equations yields the following general expressions:

$$H_y^S(z) = A_i \exp \frac{z}{\lambda_S} + B_i \exp -\frac{z}{\lambda_S},$$
$$H_y^F(z) = C_i \exp \frac{z}{\lambda_F} + D_i \exp -\frac{z}{\lambda_F}, \tag{1}$$

where the subscript of coefficients, i, specifies the superconducting layer or the ferromagnetic layer in the stack, λ_S is the superconducting penetration depth, $\lambda_F = \delta_F \Omega$ is the renormalized electromagnetic penetration depth for the ferromagnetic metal at resonance [15–17], and $\delta_F = \sqrt{i/\mu_0 \omega \sigma_F}$ is the conventional electromagnetic penetration depth into a metal with conductivity σ_F. For instance, the conductivity in our permalloy thin films, estimated at a temperature of about 5 K, $\sigma_F \approx 1.5 \times 10^6$ Ohm^{-1} m^{-1}, corresponds to an electromagnetic penetration depth of $\delta_F \approx 3$ µm at a frequency of 10 GHz. The renormalization coefficient Ω is given by the expression

$$\Omega^2 = \frac{\gamma^2 (H + H_a)(H + H_a + M_{\text{eff}}) - \omega^2}{\gamma^2 (H + H_a + M_{\text{eff}})^2 - \omega^2}, \tag{2}$$

where γ is the gyromagnetic ratio in permalloy, ω is the microwave frequency, H is the external field (aligned with the x axis in Fig. 1), H_a is the effective field of the uniaxial anisotropy aligned with the external field, and $M_{\text{eff}} = M_s - 2K_u/\mu_0 M_s$ is the effective magnetization, which accounts for the out-of-plane uniaxial anisotropy with constant K_u. Note that in this notation, the conventional Kittel formula for the ferromagnetic resonance in thin films is provided by $\Omega = 0$. Below, the coefficient Ω will be employed for the implicit derivation of ferromagnetic resonance frequencies in S-F multilayers.

At every S-F interface the following boundary conditions are fulfilled:

$$H_y^S = H_y^F,$$
$$\frac{1}{\sigma_S} \frac{dH_y^S}{dz} = \frac{1}{\sigma_F} \frac{dH_y^F}{dz}, \tag{3}$$

where $\sigma_S = i/\mu_0 \omega \lambda_S^2$ is the imaginary conductance in superconducting layers.

For the S-F-S trilayer, depicted schematically in Fig. 1, the solution of Eq. (3) together with the natural boundary conditions at the outer surfaces of the S layers, namely, $H_y^S = 0$, and in the limit $d_F \ll \lambda_F$, yields the following
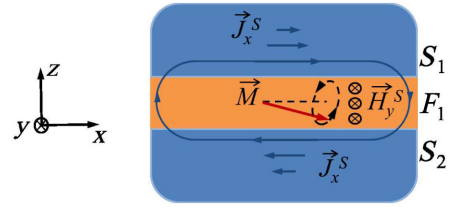

FIG. 1. A schematic illustration of the interplay between the ac magnetic field, the magnetization precession, and the superconducting currents in an S-F-S trilayer. The ferromagnetic film is magnetized along the x axis. The magnetization precession ($\vec{M}$, black arrow) at S-F interfaces induces macroscopic superconducting currents alternating in S layers along the x direction (J_x^S, blue arrows). These currents form the magnetic field H_y^S in the F layer along the y direction, in opposite phase to the precession of $\vec{M}$.

expression for ferromagnetic resonance frequency:

$$\Omega^2 = -\frac{d_F}{\lambda_S} \frac{\tanh d_{S1}/\lambda_S \tanh d_{S2}/\lambda_S}{\tanh d_{S1}/\lambda_S + \tanh d_{S2}/\lambda_S}. \tag{4}$$

As an example, the black and red curves in Fig. 2 compare the dependence of the resonance frequency on the magnetic field $f_r(H)$ in a single F layer and in an S-F-S trilayer, respectively, with the following thicknesses: $d_{F1} = 50$ nm, $d_{S1} = 150$ nm, $d_{S2} = 100$ nm, and $\lambda_S = 100$ nm. These thicknesses correspond to $\Omega^2 = -0.2$ and to the renormalized penetration depth $\lambda_F \approx 1.3$ µm at 10 GHz, which is consistent with the presumed limit of $d_F \ll \lambda_F$.

The application of the same derivation approach for the symmetric S-F-S-F-S multilayer, depicted schematically in Fig. 3, yields two resonance modes with the in-phase (acoustic mode) and the antiphase (optic mode) precession of ferromagnetic layers, respectively,

$$\Omega_a^2 = -\frac{d_F}{\lambda_S} \frac{\tanh d_{Si}/\lambda_S \coth d_{Se}/2\lambda_S}{\tanh d_{Si}/\lambda_S + \coth d_{Se}/2\lambda_S},$$
$$\Omega_o^2 = -\frac{d_F}{\lambda_S} \frac{\tanh d_{Si}/\lambda_S \tanh d_{Se}/2\lambda_S}{\tanh d_{Si}/\lambda_S + \tanh d_{Se}/2\lambda_S}, \tag{5}$$

where Se denotes external superconducting layers (S_1 and S_3 in Fig. 3), Si corresponds to the internal superconducting layer (S_2 in Fig. 3), and the thicknesses of both ferromagnetic layers are considered equal: $d_{F1} = d_{F2} = d_F$. The blue curves in Fig. 2 show acoustic and optical resonance curves $f_r(H)$ in the multilayer with the same thicknesses as in a single F layer and in an S-F-S trilayer: $d_{F1} = d_{F2} = d_F = 50$ nm, $d_{S1} = d_{S3} = d_{Se} = 150$ nm, $d_{Si} = 100$ nm, and $\lambda_S = 100$ nm.

It should be noted that the acoustic mode [Fig. 3(a)] can be thought as being formed by the global superconducting current, which circulates in external superconducting layers S_1 and S_3, while the internal superconducting layer S_2
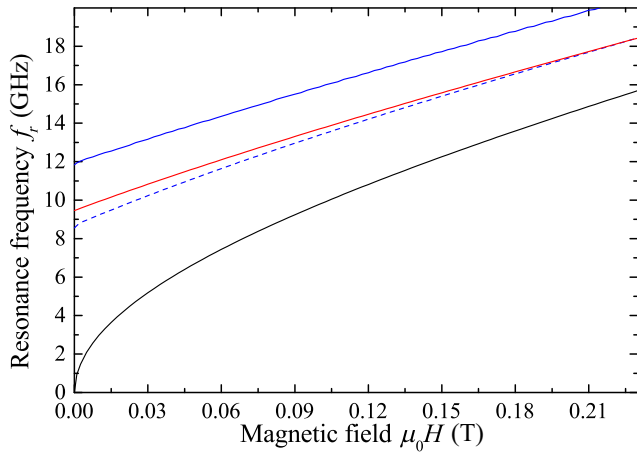
FIG. 2. The theoretical dependencies of the resonance frequency on the magnetic field $f_r(H)$ in a conventional F layer (solid black curve, Kittel formula), an *S-F-S* trilayer [solid red curve, Eq. (4)] and a symmetric *S-F-S-F-S* multilayer [solid and dashed blue curves, Eq. (5)]. The following parameters are used for the calculations: $\gamma/2\pi = 29.5$ GHz/T, $d_{F1} = d_{F2} = 50$ nm, $d_{S1} = d_{S3} = d_{Se} = 150$ nm, $d_{S2} = d_{Si} = 100$ nm, $\lambda_S = 100$ nm, $\mu_0 M_{\text{eff}} = 1$ T, and $H_a = 0$.

only screens the induced magnetic field in the conventional manner. In fact, in the limit $d_{Se} \to \infty$, the expression for Ω_a in Eq. (5) corresponds to Eq. (4) with the substitution $d_F \to 2d_F$. The optical mode [Fig. 3(b)] can be thought as the resonance in the *S-F-S* trilayer with a reduced thickness of the internal S layer: the expression for Ω_o in Eq. (5) corresponds to Eq. (4) with the substitution $d_{S2} = d_{Si}/2$. Qualitatively, it can be concluded that the optical mode is unaffected by the interaction between the F layers, while the acoustic mode gains energy due to the coupling. Interestingly, this qualitative picture is in direct contradiction to the magnetization dynamics in exchange-coupled ferromagnetic layers [18–22], where regardless of the details of the exchange interaction, the acoustic mode corresponds to the magnetization dynamics in noninteracting magnetic layers. Also, according to Fig. 2 and Eq. (5), the optical mode is observed at lower frequencies in comparison to the acoustic mode, which characterizes the coupling between the ferromagnetic layers via the superconducting layers as antiferromagnetic. In a way, such an interaction between ferromagnetic layers via superconducting currents in adjacent layers is reminiscent of the interaction of fluxons in superconductor-insulator Josephson-junction stacks [23–25].

In the general case, the resonance modes of an arbitrary *S-F* multilayer, which consists of N ferromagnetic layers and $N + 1$ superconducting layers, can be derived numerically from the set of equations given in Eq. (3) in matrix form, $[M] \times [A_n, B_n, C_n, D_n]^T = 0$, by finding frequencies
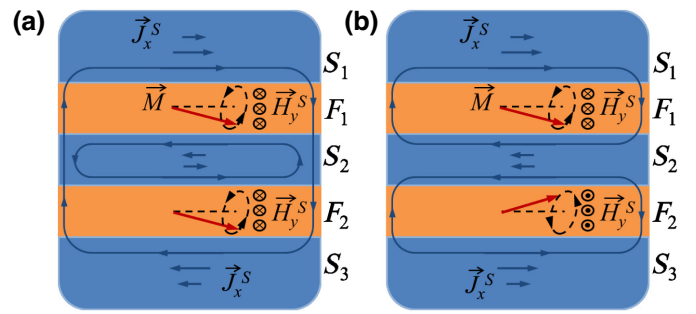

FIG. 3. A schematic illustration of the interplay between the ac magnetic field, the magnetization precession, and the superconducting currents in a symmetric *S-F-S-F-S* multilayer: (a) acoustic and (b) optical modes are formed.

ω_r that obey the expression

$$\det[M(\omega_r)] = 0. \qquad (6)$$

Experimental details and results.—Experimentally, the magnetization dynamics in *S-F* multilayers are studied by measuring the ferromagnetic resonance absorption spectrum using the vector network analyzer (VNA)−ferromagnetic resonance (FMR) approach [26–28] and the same chip layout and experimental setup as in Refs [13,14]. A series of niobium–permalloy (Py = $Fe_{20}Ni_{80}$)–niobium (Nb-Py) multilayered structures are placed directly on top of the central transmission line of a superconducting Nb waveguide. The deposition of Nb-Py multilayers is performed in a single vacuum cycle, ensuring electron transparency at the Nb-Py interfaces. A thin Si or AlO_x spacing layer is deposited between the Nb coplanar waveguide and the multilayers in order to ensure electrical insulation of the studied samples from the waveguide. Two test samples have been studied: a sample with two ferromagnetic layers, that consists of Nb(101 nm)/Py(11 nm)/Nb(41 nm)/Py(11 nm)/Nb(41 nm), referred to as SF2, and a sample with three ferromagnetic layers, that consists of Nb(101 nm)/Py(11 nm)/Nb(40 nm)/Py(11 nm)/Nb(40 nm)/Py(12 nm)/Nb(41 nm), referred to as SF3. The SF2 sample is made asymmetric on purpose in order to provide a finite dynamic susceptibility for the optical mode, which is otherwise zero and, thus, does not couple to the uniform microwave magnetic field of the transmission line.

Microwave spectroscopy of the samples was performed by measuring the transmission characteristics $S_{21}(f, H)$ in the Oxford Instruments Triton closed-cycle cryostat (base temperature 1.2 K) equipped with a home-made superconducting solenoid. The spectroscopy was performed in the field range from -0.22 T to 0.22 T, in the frequency range from 0 up to 20 GHz, and in the temperature range from 2 to 11 K. The magnetic field was applied in plane along the direction of the waveguide (see Ref. [14]). The
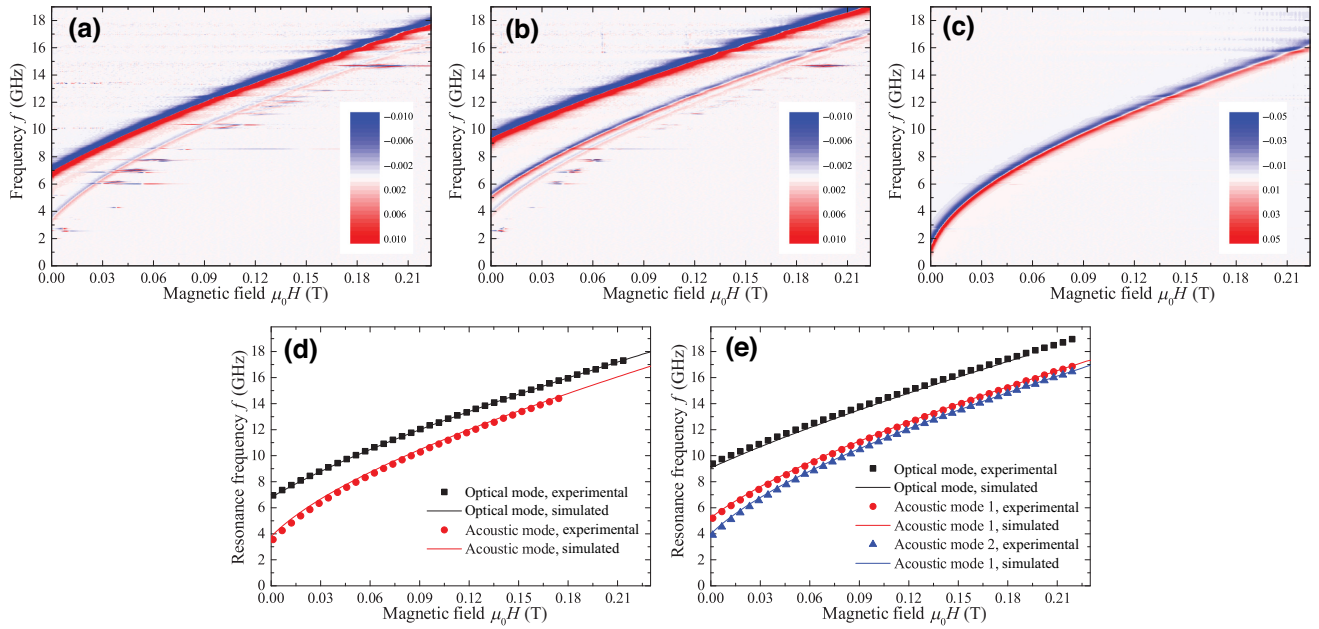
FIG. 4. (a)–(c) Differentiated transmission spectra $dS_{21}/dH(f,H)$ for samples (a) SF2 and (b) SF3 at a temperature of 2 K and (c) for sample SF2 at 8 K. Color codes are provided in the insets. (d),(e) Experimental (symbols) and theoretical (solid curves) resonance lines for samples (d) SF2 and (e) SF3 at temperatures of 2 K.

spectroscopy at various field sweeps showed no magnetic hysteresis. The FMR spectra at different temperatures were analyzed by fitting $S_{21}(f)$ characteristics at specified H and T values with the Lorentz curve and, thus, obtaining the dependencies of the resonance frequency on the magnetic field $f_r(H)$.

Figures 4(a)–4(c) demonstrate the essence of the studied phenomenon: at temperatures below the critical temperature of Nb, $T < T_c$, the transmission spectrum for sample SF2 consists of two spectral lines [Fig. 4(a)] and that for sample SF3 consists of three spectral lines [Fig. 4(b)]. At $T > T_c$ [Fig. 4(c)], the FMR spectrum for both samples is reduced to a single spectral line, which obeys the conventional Kittel formula [Eq. (2), $\Omega = 0$]. For both samples, the fit of the FMR curves at $T > T_c$ yields a negligible anisotropy field $\mu_0 H_a \approx 2$ mT, an effective magnetization $\mu_0 M_{\text{eff}} \approx 1.108$ T, which is close to typical values of the saturation magnetization of permalloy, $\mu_0 M_s \approx 1$ T, and no noticeable dependence of H_a and M_{eff} on the temperature. The temperature dependencies of the FMR spectra for both samples yield superconducting critical temperatures of $T_c = 7.7$ K for sample SF2 and $T_c = 7.9$ K for sample SF3. The critical temperature of the Nb layers is reduced in comparison to the bulk critical temperature of Nb, $T_c \approx 9$ K, due to the inverse-proximity effect [29].

At $T < T_c$ [Figs. 4(a) and 4(b)], the FMR spectrum shifts to higher frequencies and splits into spectral lines in accordance with the number of F layers in the stack. The strongest line, the acoustic mode, is observed at the highest frequencies, while the weaker lines at lower

frequencies correspond to optical modes. The resonance lines were modeled with Eq. (6), using λ_S as the fitting parameter [see Figs. 4(d) and 4(e)]. The optimum fit is obtained with $\lambda_S = 115$ nm for sample SF2 and $\lambda_S = 98$ nm for sample SF3. The obtained λ_S is slightly higher than typical values in bulk Nb (about 80 nm) due to the inverse-proximity effect [15,29]. A better fit could be obtained by considering a variation of λ_S in different S layers. Thus, the provided theoretical description of the magnetization dynamics phenomenon in arbitrary S-F multilayers is verified.

Conclusions.—To summarize, we report a study of the magnetization dynamics in S-F multilayers. Theoretical considerations supported by experiments over wide frequency, field, and temperature ranges show that the coupling between the ferromagnetic layers via the superconducting layers results in the formation of an antiferromagnetic interaction between the F layers, with a strength that depends on the thickness and superconducting properties of the S layers. This interaction between ferromagnetic layers is formed via superconducting currents and results in the formation of acoustic and optical spectral branches. These results may open up wide prospects for the application of S-F multilayers in magnonics and may also bridge magnetization dynamics phenomena with various superconducting circuits [30–32], hybrid devices [8,9], and metamaterials [33]—and, moreover, the resonance properties of S-F multilayers by changing the superconducting state of S layers optically [15,34,35] or via electric currents.

---

[1] J. Linder and J. W. A. Robinson, Superconducting spintronics, Nat. Phys. **11,** 307 (2015).

[2] O. V. Dobrovolskiy, R. Sachser, T. Bracher, T. Fischer, V. V. Kruglyak, R. V. Vovk, V. A. Shklovskij, M. Huth, B. Hillebrands, and A. V. Chumak, Magnon-fluxon interaction in a ferromagnet/superconductor heterostructure, Nat. Phys. **15,** 477 (2019).

[3] O. V. Dobrovolskiy, Q. Wang, D. Y. Vodolazov, B. Budinska, S. Knauer, R. Sachser, M. Huth, and A. I. Buzdin, Cherenkov radiation of spin waves by ultra-fast moving magnetic flux quanta, arXiv:2103.10156 (2023).

[4] I. A. Golovchanskiy, N. N. Abramov, V. S. Stolyarov, V. V. Bolginov, V. V. Ryazanov, A. A. Golubov, and A. V. Ustinov, Ferromagnet/superconductor hybridization for magnonic applications, Adv. Funct. Mater. **28,** 1802375 (2018).

[5] I. A. Golovchanskiy, N. N. Abramov, V. S. Stolyarov, V. V. Ryazanov, A. A. Golubov, and A. V. Ustinov, Modified dispersion law for spin waves coupled to a superconductor, J. Appl. Phys. **124,** 233903 (2018).

[6] I. A. Golovchanskiy, N. N. Abramov, V. S. Stolyarov, P. S. Dzhumaev, O. V. Emelyanova, A. A. Golubov, V. V. Ryazanov, and A. V. Ustinov, Ferromagnet/superconductor hybrid magnonic metamaterials, Adv. Sci. **6,** 1900435 (2019).

[7] T. Yu and G. E. W. Bauer, Efficient Gating of Magnons by Proximity Superconductors, Phys. Rev. Lett. **129,** 117201 (2022).

[8] I. A. Golovchanskiy, N. N. Abramov, V. S. Stolyarov, M. Weides, V. V. Ryazanov, A. A. Golubov, A. V. Ustinov, and M. Y. Kupriyanov, Ultrastrong photon-to-magnon coupling in multilayered heterostructures involving superconducting coherence via ferromagnetic layers, Sci. Adv. **7,** eabe8638 (2021).

[9] I. A. Golovchanskiy, N. N. Abramov, V. S. Stolyarov, A. A. Golubov, M. Y. Kupriyanov, V. V. Ryazanov, and A. V. Ustinov, Approaching Deep-Strong On-Chip Photon-To-Magnon Coupling, Phys. Rev. Appl. **16,** 034029 (2021).

[10] M. A. Silaev, Ultrastrong magnon-photon coupling, squeezed vacuum, and entanglement in superconductor/ferromagnet nanostructures, Phys. Rev. B **107,** L180503 (2023).

[11] L.-L. Li, Y.-L. Zhao, X.-X. Zhang, and Y. Sun, Possible evidence for spin-transfer torque induced by spin-triplet supercurrents, Chin. Phys. Lett. **35,** 077401 (2018).

[12] K.-R. Jeon, C. Ciccarelli, H. Kurebayashi, L. F. Cohen, X. Montiel, M. Eschrig, T. Wagner, S. Komori, A. Srivastava, J. W. Robinson, and M. G. Blamire, Effect of Meissner Screening and Trapped Magnetic Flux on Magnetization Dynamics in Thick Nb/Ni$_{80}$Fe$_{20}$/Nb Trilayers, Phys. Rev. Appl. **11,** 014061 (2019).

[13] I. A. Golovchanskiy, N. N. Abramov, V. S. Stolyarov, V. I. Chichkov, M. Silaev, I. V. Shchetinin, A. A. Golubov, V. V. Ryazanov, A. V. Ustinov, and M. Y. Kupriyanov, Magnetization Dynamics in Proximity-Coupled Superconductor-Ferromagnet-Superconductor Multilayers, Phys. Rev. Appl. **14,** 024086 (2020).

[14] I. A. Golovchanskiy, N. N. Abramov, O. V. Emelyanova, I. V. Shchetinin, V. V. Ryazanov, A. A. Golubov, and V. S. Stolyarov, Magnetization Dynamics in Proximity-Coupled Superconductor-Ferromagnet-Superconductor Multilayers. II. Thickness Dependence of the Superconducting Torque, Phys. Rev. Appl. **19,** 034025 (2023).

[15] M. A. Silaev, Anderson-Higgs Mass of Magnons in Superconductor-Ferromagnet-Superconductor Systems, Phys. Rev. Appl. **18,** L061004 (2022).

[16] M. Kostylev, Strong asymmetry of microwave absorption by bilayer conducting ferromagnetic films in the microstrip-line based broadband ferromagnetic resonance, J. Appl. Phys. **106,** 043903 (2009).

[17] N. S. Almeida and D. L. Mills, Eddy currents and spin excitations in conducting ferromagnetic films, Phys. Rev. B **53,** 12232 (1996).

[18] D. S. Schmool and J. M. Barandiaran, Ferromagnetic resonance and spin wave resonance in multiphase materials: Theoretical considerations, J. Phys.: Condens. Matter **10,** 10679 (1998).

[19] J. Lindner and K. Baberschke, *In situ* ferromagnetic resonance: an ultimate tool to investigate the coupling in ultrathin magnetic films, J. Phys.: Condens. Matter **15,** R193 (2003).

[20] S. M. Rezende, A. Azevedo, and R. L. Rodriguez-Suarez, Introduction to antiferromagnetic magnons, J. Appl. Phys. **126,** 151101 (2019).

[21] I. A. Golovchanskiy and V. S. Stolyarov, Magnetization and spin resonances in helical spin systems, J. Appl. Phys. **131,** 053901 (2022).

[22] I. A. Golovchanskiy, N. N. Abramov, V. A. Vlasenko, K. Pervakov, I. V. Shchetinin, P. S. Dzhumaev, O. V. Emelyanova, D. S. Baranov, D. S. Kalashnikov, K. B. Polevoy, V. M. Pudalov, and V. S. Stolyarov, Antiferromagnetic resonances in twinned EuFe$_2$As$_2$ single crystals, Phys. Rev. B **106,** 024412 (2022).

[23] T. Holst, J. B. Hansen, N. Grnbech-Jensen, and J. A. Blackburn, Phase locking between Josephson soliton oscillators, Phys. Rev. B **42,** 127 (1990).

[24] S. Sakai, P. Bodin, and N. F. Pedersen, Fluxons in thin-film superconductor-insulator superlattices, J. Appl. Phys. **73,** 2411 (1993).

[25] A. V. Ustinov and H. Kohlstedt, Interlayer fluxon interaction in Josephson stacks, Phys. Rev. B **54,** 6111 (1996).

[26] I. Neudecker, G. Woltersdorf, B. Heinrich, T. Okuno, G. Gubbiotti, and C. Back, Comparison of frequency, field, and time domain ferromagnetic resonance methods, J. Magn. Magn. Mat. **307,** 148 (2006).

[27] S. S. Kalarickal, P. Krivosik, M. Wu, C. E. Patton, M. L. Schneider, P. Kabos, T. J. Silva, and J. P. Nibarger, Ferromagnetic resonance linewidth in metallic thin films: Comparison of measurement methods, J. Appl. Phys. **99,** 093909 (2006).

[28] Y.-C. Chen, D.-S. Hung, Y.-D. Yao, S.-F. Lee, H.-P. Ji, and C. Yu, Ferromagnetic resonance study of thickness-dependent magnetization precession in $Ni_{80}Fe_{20}$ films, J. Appl. Phys. **101**, 09C104 (2007).

[29] J. Aarts, J. M. E. Geers, E. Brück, A. A. Golubov, and R. Coehoorn, Interface transparency of superconductor/ferromagnetic multilayers, Phys. Rev. B **56**, 2779 (1997).

[30] S. E. Barnes, M. Aprili, I. Petkovic, and S. Maekawa, Ferromagnetic resonance with a magnetic Josephson junction, Supercond. Sci. Technol. **24**, 024020 (2011).

[31] S. Mai, E. Kandelaki, A. F. Volkov, and K. B. Efetov, Interaction of Josephson and magnetic oscillations in Josephson tunnel junctions with a ferromagnetic layer, Phys. Rev. B **84**, 144519 (2011).

[32] I. A. Golovchanskiy, N. N. Abramov, V. S. Stolyarov, O. V. Emelyanova, A. A. Golubov, A. V. Ustinov, and V. V. Ryazanov, Ferromagnetic resonance with long Josephson junction, Supercond. Sci. Technol. **30**, 054005 (2017).

[33] A. Pimenov, A. Loidl, P. Przyslupski, and B. Dabrowski, Negative Refraction in Ferromagnet-Superconductor Superlattices, Phys. Rev. Lett. **95**, 247009 (2005).

[34] I. S. Veshchunov, W. Magrini, S. V. Mironov, A. G. Godin, J.-B. Trebbia, A. I. Buzdin, P. Tamarat, and B. Lounis, Optical manipulation of single flux quanta, Nat. Comm. **7**, 12801 (2016).

[35] W. Magrini, S. V. Mironov, A. Rochet, P. Tamarat, A. I. Buzdin, and B. Lounis, *In-situ* creation and control of Josephson junctions with a laser beam, Appl. Phys. Lett. **114**, 142601 (2019).